Mechanical tomography of an archaeal lemon-shaped virus reveals membrane-like fluidity of the capsid and liquid nucleoprotein cargo

Miguel Cantero, Virginija Cvirkaite-Krupovic, Mart Krupovic, Pedro de Pablo

PNAS RESEARCH ARTICLE | BIOPHYSICS AND COMPUTATIONAL BIOLOGY

Mechanical tomography of an archaeal lemon-shaped virus reveals membrane-like fluidity of the capsid and liquid nucleoprotein cargo

Miguel Cantero[a], Virginija Cvirkaite-Krupovic[b], Mart Krupovic[b], and Pedro J. de Pablo[a,c,1]

Edited by Tatyana Polenova, University of Delaware, Newark, DE; received May 8, 2023; accepted September 8, 2023 by Editorial Board Member Michael F. Summers

Archaeal lemon-shaped viruses have unique helical capsids composed of highly hydrophobic protein strands which can slide past each other resulting in remarkable morphological reorganization. Here, using atomic force microscopy, we explore the biomechanical properties of the lemon-shaped virions of Sulfolobus monocaudavirus 1 (SMV1), a double-stranded DNA virus which infects hyperthermophilic (~80 °C) and acidophilic (pH ~ 2) archaea. Our results reveal that SMV1 virions are extremely soft and withstand repeated extensive deformations, reaching remarkable strains of 80% during multiple cycles of consecutive mechanical assaults, yet showing scarce traces of disruption. SMV1 virions can reversibly collapse wall-to-wall, reducing their volume by ~90%. Beyond revealing the exceptional malleability of the SMV1 protein shell, our data also suggest a fluid-like nucleoprotein cargo which can flow inside the capsid, resisting and accommodating mechanical deformations without further alteration. Our experiments suggest a packing fraction of the virus core to be as low as 11%, with the amount of the accessory proteins almost four times exceeding that of the viral genome. Our findings indicate that SMV1 protein capsid displays biomechanical properties of lipid membranes, which is not found among protein capsids of other viruses. The remarkable malleability and fluidity of the SMV1 virions are likely necessary for the structural transformations during the infection and adaptation to extreme environmental conditions.

archeal virus | membrane fluididty | physical virology | Atomic Force Microscopy

Significance

Lemon-shaped archaeal viruses are found in some of the most extreme environments (80 °C, pH ~2). They undergo dramatic architectural rearrangement into tubular structures that could be facilitated by their unique helical structure built of seven strands of major capsid protein. Little is known about the mechanical properties compatible with this alteration and their ability to thrive in such environments. Our experiments reveal that lemon-shaped virions withstand deformations of 80%, collapsing wall-to-wall without damage. Our data suggest a protein shell with membrane-like fluidity and a liquid genomic cargo that only fills ~11% of the virion internal volume. These features are in stark contrast with those known for other viruses with protein capsids, stressing the interplay between mechanics, structure, and function.

Viruses have evolved to prosper in almost any ecological niche where living cells can be found, including some of the most severe ecosystems. The microbial communities in extreme environments are typically dominated by archaea, which harbor a highly diverse virome, characterized by unique virion morphologies not observed among viruses of bacteria or eukaryotes (1–4). Two of the most widespread archaeal virus groups correspond to helical filamentous viruses classified into the realm *Adnaviria* (5) and viruses with lemon-shaped (or spindle-shaped) virions (6–8), respectively. Both filamentous and lemon-shaped viruses are ancient, thought to have been already associated with the last archaeal common ancestor (9).

How archaeal viruses endure the extreme physicochemical conditions, especially, when outside of the host cell, remains poorly understood. One of the molecular adaptations to high temperatures described for filamentous adnaviruses involves storage of the genomic double-stranded (ds) DNA in the virions in A-form conformation (10). This is achieved through extensive interactions between the major capsid protein (MCP) subunits and the viral genome (10, 11). In some adnaviruses, the nucleocapsid is covered by a thin lipid envelope (12, 13), which is believed to provide an additional layer of protection against the acidic environment of their natural habitats (2).

By contrast, lemon-shaped viruses display a radically different virion organization compared to adnaviruses, and the details of their resilience to high temperatures and acidic pH remain unknown. Cryo-EM structure of the Sulfolobus monocaudavirus 1 (SMV1) and Acidianus two-tailed virus (ATV), both members of the family *Bicaudaviridae* (14, 15) infecting archaea that thrive in terrestrial hot springs (~80 °C, pH 2 to 3), revealed that their lemon-shaped capsids are not enveloped and represent a helical assembly constructed from seven strands of a highly hydrophobic MCP (16). Upon induction of genome ejection, the regular lemon-shaped capsids undergo dramatic architectural transformation into tubular structures (16). A similar architectural change has been observed when virions were incubated at high temperatures (17). The lemon shape of the virion results from the variations in the diameter of the virion helix, which increases from the tips to the center of the virus particle. The capsid is organized in such a way that the hydrophilic regions of the MCP are facing the lumen and exterior of the capsid, whereas

Author contributions: M.C., V.C.-K., M.K., and P.J.d.P. designed research; M.C. and V.C.-K. performed research; V.C.-K. and M.K. contributed new reagents/analytic tools; P.J.d.P. and M.C. analyzed data; and M.C., V.C.-K., M.K., and P.J.d.P. wrote the paper.

The authors declare no competing interest.

This article is a PNAS Direct Submission. T.P. is a guest editor invited by the Editorial Board.

[1]To whom correspondence may be addressed. Email: p.j.depablo@uam.es.

This article contains supporting information online at https://www.pnas.org/lookup/suppl/doi:10.1073/pnas.2307717120/-/DCSupplemental.

Published October 12, 2023.

the hydrophobic core mediates all the intra- and interstrand interactions in the capsid shell, allowing seamless sliding of the hydrophobic MCP strands past each other without disrupting the capsid integrity (16). The helical virion organization was initially recognized for a distantly related bicaudavirus Acidianus tailed spindle virus (ATSV) and the necessity for the sliding of virion strands against each other during genome externalization was predicted (18). However, the molecular underpinning of this process could not be envisioned at the time because a wrong structural protein was thought to be responsible for the capsid shell formation. The prediction that virion organization determined for SMV1 and ATV also extends to archaeal bacilli-form and smaller lemon-shaped viruses (16) was subsequently confirmed in the case of viruses of the *Fuselloviridae* family (19).

In a way, the capsid shell of bicaudaviruses can be regarded as a unique "protein membrane," with a highly hydrophobic core sandwiched between hydrophilic termini. However, whether such capsids possess biomechanical properties, such as fluidity and softness, akin to those of lipid-based membranes or are more like other protein capsids remains unknown. Interestingly, theoretical investigations (20) suggested that ATV and ATV-like capsids are anisotropic viscoelastic materials, which would facilitate the experimentally observed architectural virion rearrangements. Understanding the properties of the lemon-shaped virions is of great interest not only from a fundamental point of view but also from a biotechnological perspective and could stimulate the development of next-generation biomaterials for biomedicine and nanotechnology. Indeed, SMV1 particles have already shown promise as potential nanocarriers (21).

Mechanics is an essential property of macromolecular assemblies (22) and virus capsids are not an exception (23). For instance, tailed bacteriophages actively package dsDNA genomes into their capsids, subjecting them to high internal pressures (up to 90 atmospheres) (24, 25), which is then used during the first stages of DNA translocation into the host (26, 27). Therefore, their capsids are endowed with extraordinary robustness to support such mechanical stress (28). Atomic force microscopy (AFM) has emerged as a powerful method to study the structural and mechanical properties of viral particles under physiological conditions (29). AFM analysis of bacterial and eukaryotic viruses with proteinaceous capsids, such as human adenovirus, bacteriophages lambda, P22 and phi29, have demonstrated a direct interplay between the biomechanical properties and functionality of the viral particles (28). In human adenovirus, the stiffness and mechanical disassembly are intimately related to the condensation state of the viral genome and its ability to diffuse from semidisrupted particles to the nuclear pore (30). Mechanical properties also depend on the maturation state of the virus capsid (23) and the complexity of the virus particle, especially in viruses with multilayered capsids (31). All previously studied viruses with protein capsids have been found to behave almost as elastic linear springs, with capsid shells demonstrating fragile fracture (32). By contrast, enveloped viruses, such as influenza and coronaviruses (33–35), are much softer, with measured stiffness values being 10 times lower than for protein capsids. However, none of the extremophilic archaeal viruses have been studied from a biomechanics perspective.

Here, we explore the biomechanical properties of the SMV1 capsids using AFM and assess their stiffness, resistance to cyclic loading (mechanical fatigue), and reversible morphological transformation under different loading forces. In addition, we performed mechanical tomography and dehydration studies that provided insights into the physical properties and packing fraction of the SMV1 cargo. We show that the lemon-shaped virion of SMV1 displays exotic biomechanical properties, combining the extreme malleability of the protein capsid with the remarkable fluidity of the nucleoprotein cargo, unexpected in other protein capsid-containing viruses.

Results

Topography of SMV1 Virions. The morphological diversity of purified SMV1 virions includes particles ranging from tailless lemon-shaped capsids to particles with one or two tubular tails protruding from the lemon-shaped body (Fig. 1*A*). This diversity of shapes could be also observed with AFM following the adsorption of the SMV1 to the highly oriented pyrolytic graphite (HOPG) surface (Fig. 1*B* and *SI Appendix*, Fig. S1). Fig. 1*C* shows the details of one SMV1 particle where a single tail (top right) can be observed.

Because the measurement of the virion width can be affected by tip dilation (36), the height of the virus particles (37) is typically considered to more accurately represent the virion diameter (29). The height distribution of ~750 particles (Fig. 1*D*) revealed the diameter of the SMV1 virions to be ~75 nm, with a dispersion of tens of nm, reflecting the pleomorphic nature of the lemon-shaped particles and their deformation on the surface (37). This result is compatible with the diameter of SMV1 particles measured from negatively stained SMV1 virions observed by transmission electron microscopy (TEM) (Fig. 1 *A* and *D*).

Changes in Virion Stiffness and Topography under Punctual Loading Forces. To study the mechanical properties of SMV1 virions, we performed a series of indentation experiments on the same virus particle (Fig. 2 *A* and *B*) and plotted the corresponding force-indentation curves (FIC; Fig. 2*C*). Each FIC presents the data of punctual deformation of a virion inflicted at the particle apex, where the indentation force is recorded as a function of the virus deformation (23, 28, 38). The typical FIC measurements performed on SMV1 particles begin with an elastic deformation of the virion during the first ~20 nm of indentation (Fig. 2*C*), which corresponds to a spring constant value (stiffness) of 0.01 N/m (*SI Appendix*, Fig. S2*A*).

Upon further indentation from 20 to 60 nm, the slope of the FIC decreased, until the AFM tip reached the surface of the substrate. Subsequent topographies of the SMV1 particle after performing consecutive FIC experiments (*SI Appendix*, Fig. S2*B*) with increasing forces (up to 10 nN) did not reveal any alteration of the virion structure (Fig. 2*B*). Consecutive indentations had limited effect on the virion height (Fig. 2*D* and Movie S1). Collectively, these data demonstrate that SMV1 has a remarkably soft virion, largely devoid of fragile fracture and capable of withstanding successive deformations without evident damage.

Stress Evolution and Mechanical Tomography. To further explore the biomechanical properties of the SMV1 virions, we carried out the cyclic loading experiment, during which the virions are imaged consecutively applying forces of a few hundreds of pN (39). In contrast to other viruses with protein capsids, SMV1 can be mechanically probed tens of times at constant force without showing any alteration (*SI Appendix*, Fig. S3 *A* and *B* and Movie S2). We also stressed the virus particles by cyclically alternating high and low forces (Fig. 3 and *SI Appendix*, Fig. S3*C* and Movies S3 and S4). For instance, Fig. 3 *A*, *#1* shows an intact SMV1 particle which has been imaged at a force of 100 pN. The same virus particle was subsequently subjected to 200 pN (Fig. 3 *A*, *#2*), showing conspicuous structural changes and deformation. However, when the force was set back to 100 pN (Fig. 3 *A*, *#3*), the virus topography reverted to the one observed at the onset of the experiment (#1). Applying an even higher force of 500 pN

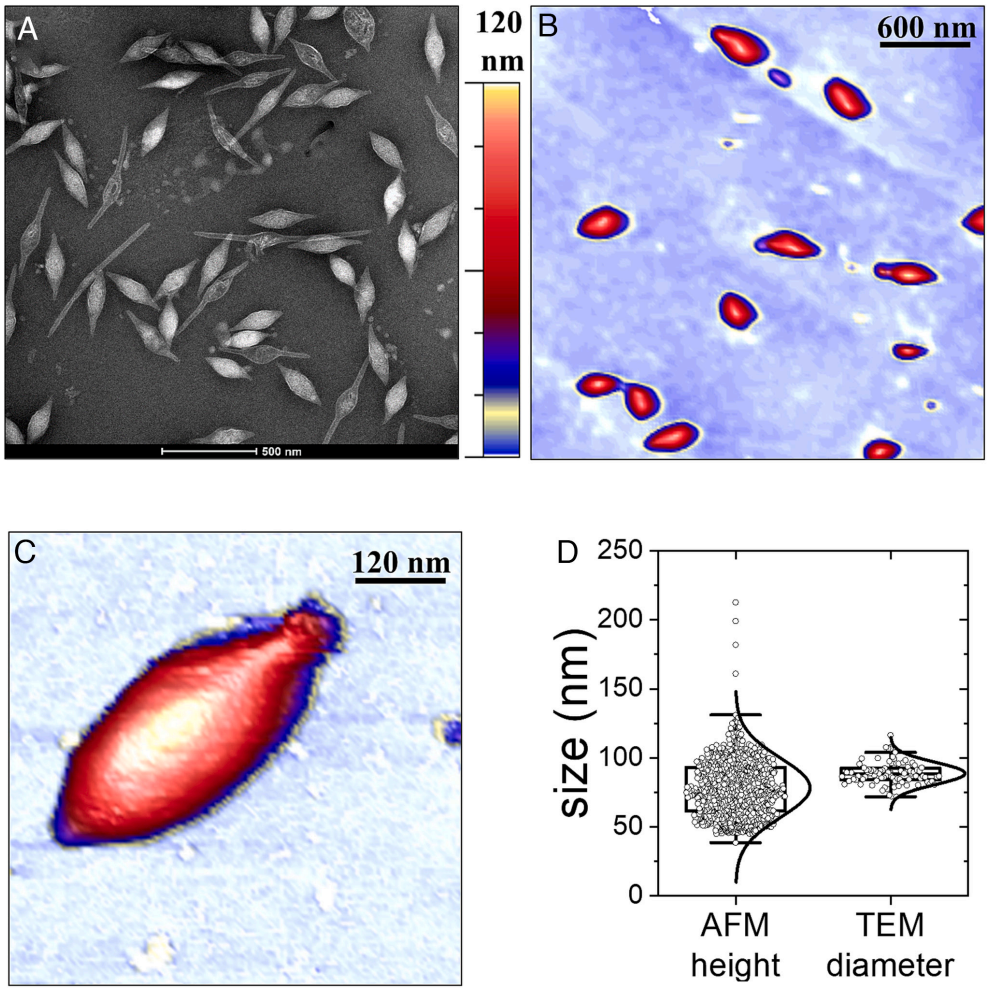

Fig. 1. SMV1 topography. (*A*) TEM micrograph of SMV1 particles. (*B*) SMV1 particles on HOPG observed by AFM. (*C*) SMV1 particle showing details about the tails and body. (*D*) Comparison between the AFM height of the particles and their diameter of TEM data.

(Fig. 3 *A*, *#4*) resulted in more pronounced virion deformation and shrinkage in the lateral dimension compared to the virion subjected to the 200 pN force (Fig. 3 *A*, *#2*). Strikingly, when the imaging force was set back to 100 pN, the virion regained its initial appearance (Fig. 3 *A*, *#5* and *Bottom Right*). This ability to recover is a consistent, inherent property of the SMV1 virions, which was evidenced in ~10 particles during nine consecutive loading cycles with forces increasing up to 1,100 pN (Fig. 3*B*). Remarkably, SMV1 particles can reach a maximum strain of 80% at 800 pN (Fig. 3*B*) with little signs of structural alteration, as revealed by the topographical profiles obtained at each force (Fig. 3 *A*, *Bottom Right*). Any increment of the force beyond this value does not achieve further virus deformation (Fig. 3*B*). These results indicate that both capsid and cargo are capable of large reversible deformation without breakage.

Fig. 4 *A* and *B* show the topography of the same SMV1 particle at 100 pN and 1,100 pN, respectively. These numbers mark the lowest and highest values of the forces used, which induce gradual deformations of the virus particle (Fig. 4*C*). When using a force of 1,100 pN, the virion appears laterally shrunken and vertically deformed, revealing a flat area (circle in Fig. 4 *B* and *C*, light blue) which accounts for ~20% of the virion surface. Fig. 4*D* shows evidence of the height change induced by 800 pN at the plateau region for several virus particles.

Dehydration Leads to Genome Externalization, Decreasing SMV1 Volume. Upon adsorption to the surface, the volume of virus particles reduces due to desiccation, which sometimes results in genome ejection (40). Notably, when the DNA is completely externalized, the virus particle collapses wall to wall. However, when the DNA is not ejected, the virus particles only decrease in volume due to dehydration (35, 40). Other than volume reduction, the topography of the SMV1 particles revealed intact and flat structures (Fig. 5*A*). Upon desiccation, ~50% of the SMV1 virions are intact (Fig. 5*B*, bottom virus), although the height is reduced from 80 nm in hydrated state to 50 nm after desiccation (Fig. 5*C*). The other 50% of SMV1 particles undergo genome ejection and appear collapsed wall-to-wall (Fig. 5*B*, top virus), presenting a height of 11.5 nm (Fig. 5*C*). This value is compatible with two stacked SMV1 capsid walls (16). Considering that in these collapsed particles, most of the genome has been ejected (Fig. 5*B*, top virus), we envisage that the differences between the heights of the intact dehydrated SMV1 and the collapsed particles (Fig. 5*C*, ~38 nm) correspond to the genomic cargo. The analysis of the SMV1 volumes shows a median of 2.5×10^6, 7.8×10^5, and 5.4×10^5 nm^3 for hydrated, dry intact, and dry flat particles, respectively (Fig. 5*D*). These data indicate that after desiccation, the major determinant for the volume decrease observed in flat particles corresponds to the cargo externalization.

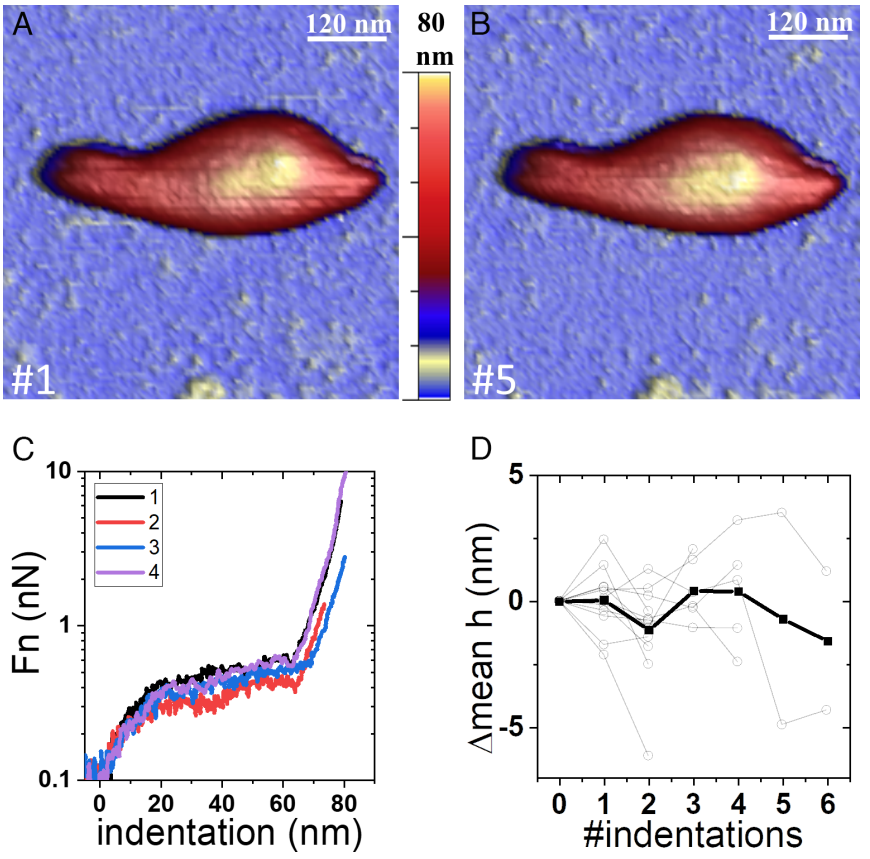

Fig. 2. Evolution of stiffness and topography under consecutive single indentations. (*A*) Initial AFM image of SMV1 before indentation. (*B*) Topography of the previous virus after four indentations. (*C*) Consecutive FICs performed on the same SMV1 particle. (*D*) Height variation evolution of 5 SMV1 particles (gray) showing that the virus particles remain mainly intact (average in black) within ~5% of the average height.

Discussion

Here, we explored the biomechanical properties of the extremophilic archaeal virus SMV1. Our measurements of elasticity indicate that the protein capsid of SMV1 (16) has a stiffness as low as 0.01 N/m (Fig. 2*B* and *SI Appendix*, Fig. S2), which is ~1/30 of the stiffness measured for mesophilic viruses with protein capsids such as adenovirus (0.6 N/m) (41, 42) or minute virus of mice (*Parvoviridae;* 0.58 N/m) (43). Furthermore, the SMV1 spring constant is not only considerably lower than those determined for enveloped viruses such as influenza (0.02 N/m), HIV-1 (0.2 N/m), SARS-CoV-2 (0.013 N/m) or internal membrane containing viruses, such as PRD1 (0.02 N/m) (33, 34, 44, 45), but also up to 10 times lower than the stiffness of membrane vesicles with and without integral proteins (46–48). However, SMV1 and other lemon-shaped virions do not contain an external or internal

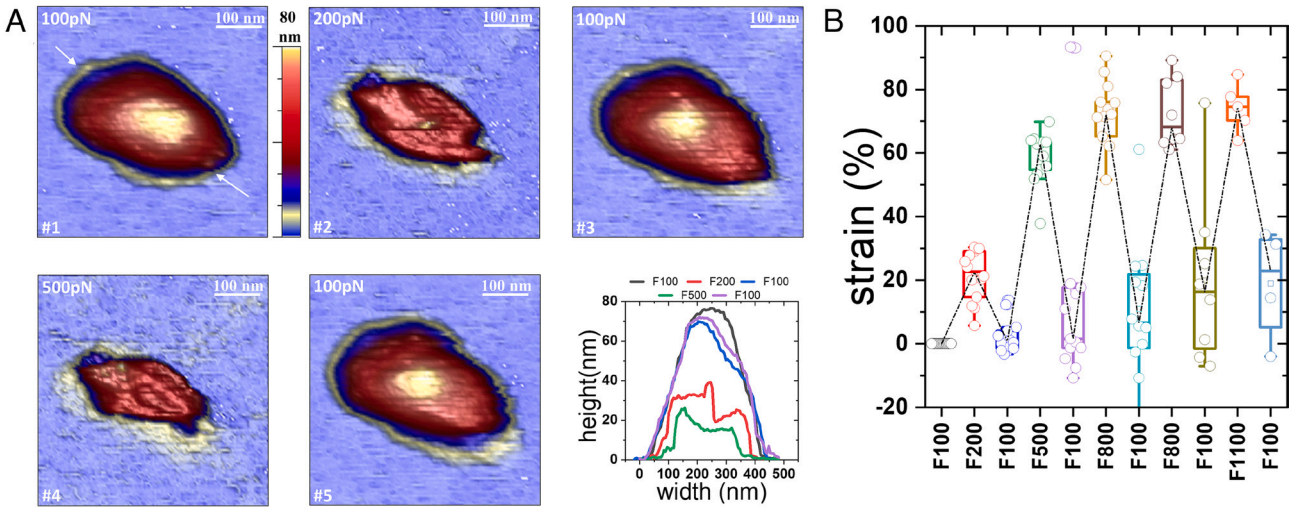

Fig. 3. Mechanical fatigue of SMV1 particles with alternated force values. (*A*) Topography evolution of SMV1 particle while scanning the particle consecutively with alternated periodic forces. The applied force is shown in the upper left corner of each frame. The last panel (*Bottom Right*) shows the evolution of the profile marked with arrows in *A*. #1 for each force. (*B*) Strain evolution for several SMV1 virions. The strain was calculated as the coefficient of the maximum height at each force divided by the initial maximum height at 100 pN. The color code is the same as in the profiles panel of *A*.

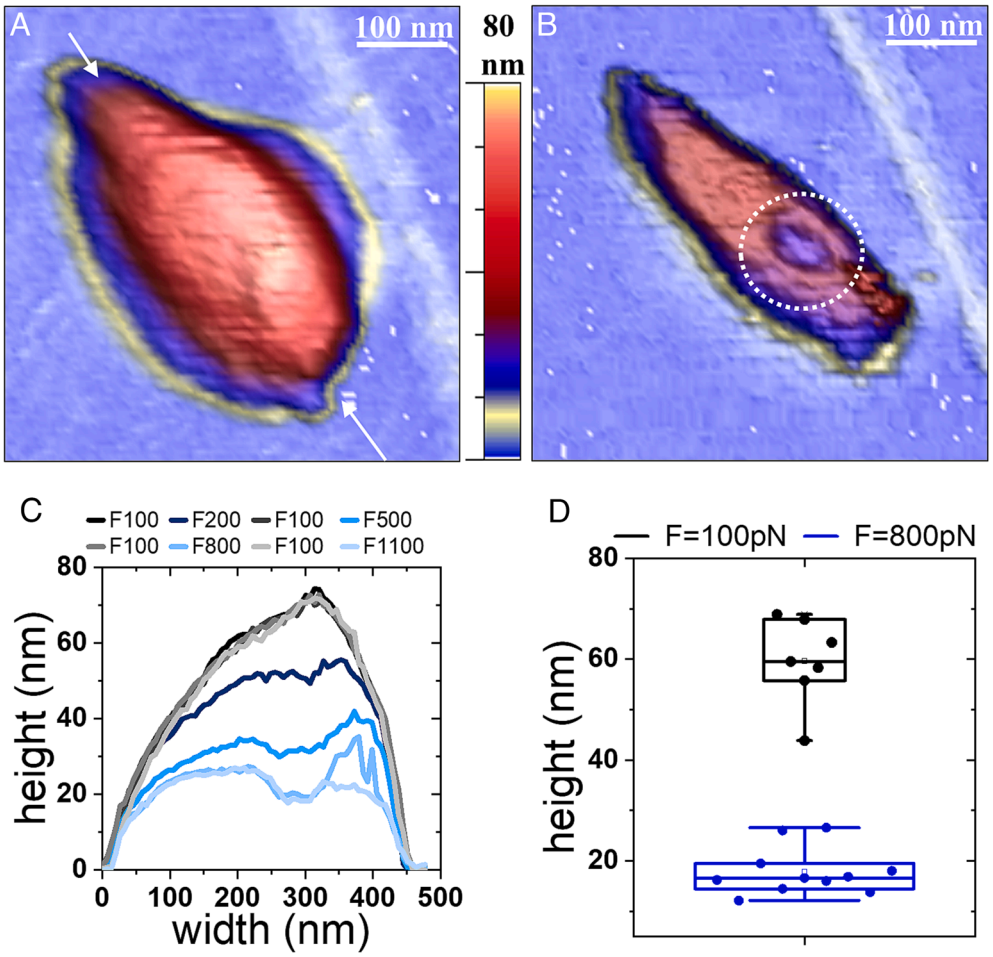

Fig. 4. Squeezing SMV1. (*A*) Topography of SMV1 at 100 pN. (*B*) Topography of the same particle obtained at 1,100 pN. The white circle marks the plateau where the maximum deformation occurs. (*C*) Topo profiles at increasing forces were obtained between the arrows of (*A*). (*D*) Box plot showing the virus height for low (black) and high forces (blue) for several viruses.

membrane layer (16, 18, 19), suggesting that the protein capsid of SMV1 exhibits mechanical properties akin to those of lipid membranes (49) (*SI Appendix*, Table S1). In addition, the contours of the force curves (Fig. 2*C*) are very different compared to those obtained for viruses with fragile protein capsids (*SI Appendix*, Fig. S4, black line) (23, 50, 51), but similar to those reported for membrane vesicles (*SI Appendix*, Fig. S4, red line) (46, 47, 52) and foam-filled tubes (53), although with a stiffness about 10 times lower.

Similar to lipid vesicles (47), SMV1 particles can withstand large deformations without breaking. Fig. 2*B* shows that SMV1 particles retain the same height and shape after five indentations, reaching 80 nm of deformation at 10 nN (Fig. 2*C*). Since the height of the SMV1 particles is around 80 nm, this means that the tip goes all the way down across the virus structure without inducing permanent breakage. Consecutive imaging of SMV1 with alternating low/high forces informs about the deformation of every pixel on the virion surface under mechanical stress (Fig. 3*A*). Such mechanical tomography reveals that the virus particle decreases/increases both the height and lateral dimensions in a cyclical way, without showing any signature of structural disruption (Fig. 3*B*). Every time the AFM tip is deforming a pixel during the imaging process, the material of the virus, both the external capsid and the internal cargo, yields and accommodates reversibly to the mechanical stress induced by the AFM tip (Figs. 4 and 6). Interestingly, for a force higher than 0.8 nN, the particle does not deform any further (Figs. 3*B* and 4*C*), revealing a plateau in the center of the virus body (Fig. 4*B*, dashed circle). The height of this plateau measured for various virus particles (n = 11) was determined to be 17 ± 5 nm (Fig. 4*D*). Given that the wall thickness of the SMV1 capsid is ~7 nm (16), the plateau likely represents a capsid region collapsed wall-to-wall, largely devoid of internal cargo in that region. This fact suggests that under the pressure exerted by the AFM tip, the virus contents flow and can migrate to other parts of the capsid lumen (Fig. 6*B*). However, when the AFM tip pushes outside the plateau, the internal cargo leaves the region partially, although the strain is still reaching about 70% (Fig. 4*C*, light blue). The AFM tip hits the virion ~3,000 times per frame with jumping mode (54), where a force curve is performed at every pixel of the virus particle during ~5 ms (39). Since the maximum virus deformation is about 50 nm (Fig. 4*B*), it is possible to estimate that the virus cargo moves at a speed of the order of 10 nm/ms inside the capsid lumen when it is probed with the AFM tip. This result indicates that SMV1 cargo, including DNA and proteins (16), has a fluidic behavior. In many bacteriophages and other viruses with protein capsids, the virion core is condensed and organized into layers (55), showing a Young's modulus ~1 MPa in a semisolid state (42, 56). Cryo-EM analysis of the bicaudavirus virions showed that the lumen of the virions is homogeneously filled with unstructured material (16, 18). Our data suggest that a nucleoprotein core can flow and be redistributed within the lumen every time the AFM deforms the SMV1

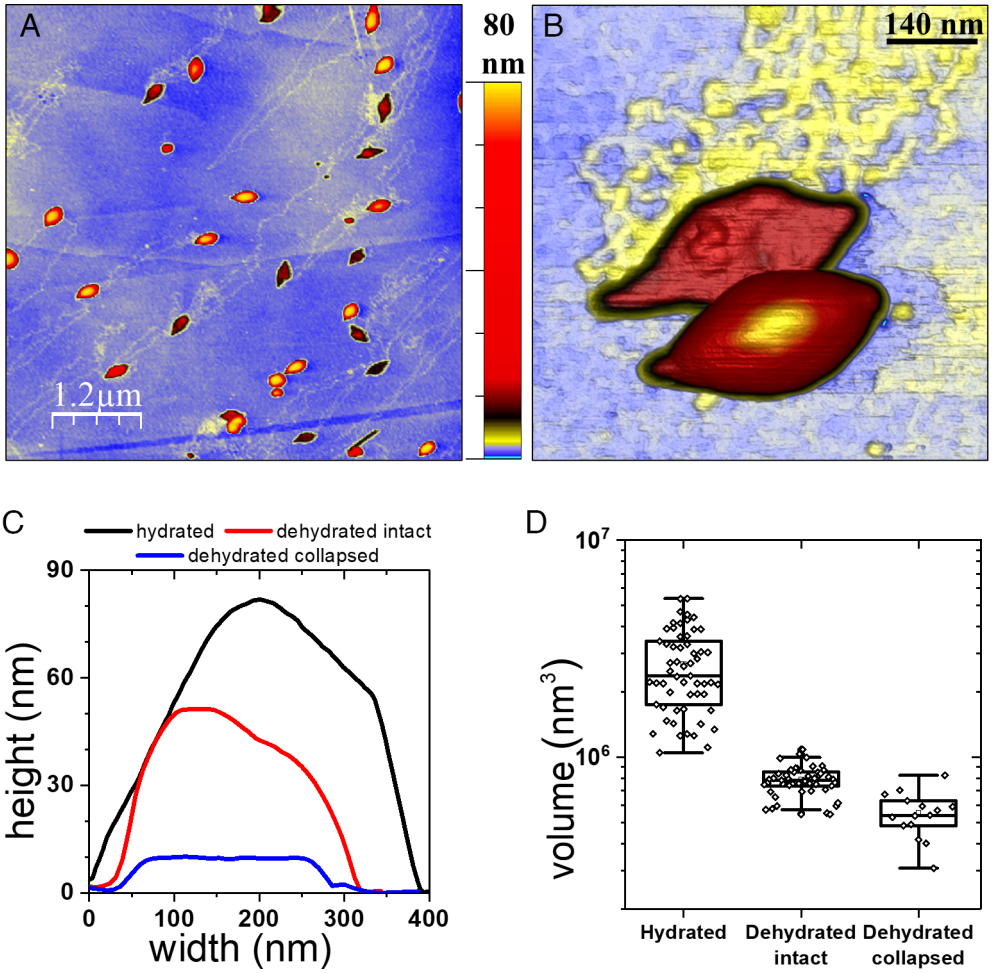

Fig. 5. Dehydration of SMV1. (*A*) Large area image (6 × 6 μm^2) after dehydration of SMV1 particles adsorbed on HOPG where the ejected DNA can be seen like yellow fibers. (*B*) Close topography (800 × 800 nm^2) showing wall-to-wall collapsed (*Up*) and intact (*Bottom*) viruses, the ejected cargo is in yellow. The color scale at the center works for *A* and *B*. (*C*) Profiles of intact hydrated, intact dehydrated, and wall-to-wall collapsed dehydrated virus (black, red, and blue, respectively). (*D*) Box chart of volume for hydrated, dehydrated intact, and dehydrated collapsed virus. Each data point corresponds to a single particle.

structure (Fig. 6). Extreme fluidity of the SMV1 nucleoprotein cargo suggests that the latter is neither solid nor crystalline, unlike in other studied viruses (55). In fact, at maximum stress, the apparent volume decreases by ~88% of the value obtained at low force (Fig. 4*B*), indicating that just 12% of the SMV1 structure does not yield under mechanical stress.

The packing fraction indicates the portion of volume that the viral genome occupies inside the capsid lumen. Viruses with icosahedral capsids and highly condensed genomes, which induce internal pressures of tens of atmospheres (25, 26, 42, 57, 58), exhibit packing fractions close to 50% (59). In a rough approximation that considers the nucleic acid molecules as cylinders, and knowing the internal volume of virus capsids, it is possible to estimate that the minute virus of mice, bacteriophage φ29, and lambda phage present packing fractions of 46%, 44%, and 34%, respectively. These viruses exhibit brittle fracture (*SI Appendix*, Fig. S4) under mechanical deformation and their cargoes are known to be quite rigid (42, 55). What is the packing fraction of the cargo within the SMV1 capsid lumen and is it compatible with the cargo's extreme fluidity? Very little is known about the nature, organization, and physical state of the SMV1 cargo. Dehydration data (Fig. 5) help to roughly estimate the packing fraction of the SMV1 core. If the volume reduction from intact ($V_i \approx 7.8 \times 10^5$ nm^3) to flat dry SMV1 particles ($V_f \approx 5.4 \times 10^5$ nm^3) is due to the cargo release (Fig. 5) (40), the coefficient V_f/V_i is ~70%, which means that 30% of the intact SMV1 dehydrated volume corresponds to the released cargo ($V_c \approx V_i - V_f = 2.4 \times 10^5$ nm^3). It has been suggested that dsDNA strands exhibit similar diameter in both liquid and air conditions when imaged with AFM (60), without significant change of volume upon dehydration. Although the cargo is homogeneously distributed within the capsid lumen, both mechanical tomography and dehydration indicate that desiccation compacts this cargo because of the capillary forces present during the last stages of desiccation (40). Therefore, it is possible to assume that the value of compacted genomic cargo (V_c) in hydrated SMV1 particles is very similar to that in dry particles. Hence, a lower limit to the packing fraction for SMV1 can be estimated with the coefficient between the volume of hydrated SMV1 ($V_h \sim 2.3 \times 10^6$ nm^3, Fig. 5*D*) and V_c, i.e., $V_c/V_h \approx 0.11$ (~11%). SMV1 packs 48,775 bps of dsDNA (61), that if it is considered as a cylinder of 1.1 nm in diameter, results in a volume of $V_{DNA} = 6.4 \times 10^4$ nm^3. Therefore, the packing fraction of just the dsDNA would be $V_{DNA}/V_h = 0.027$ (~3%). The comparison of this value with our results indicates that SMV1 packs accessory proteins, in agreement with the previous results (16, 61, 62). Our data indicate that the accessory proteins in the nucleoprotein cargo of SMV1 outnumber the genomic dsDNA with a factor of ~11/3 = 3.7. Consistent with this result, the major virion protein, which for a long time was assumed to represent the major capsid protein of bicaudaviruses (6, 15, 18, 63), turned

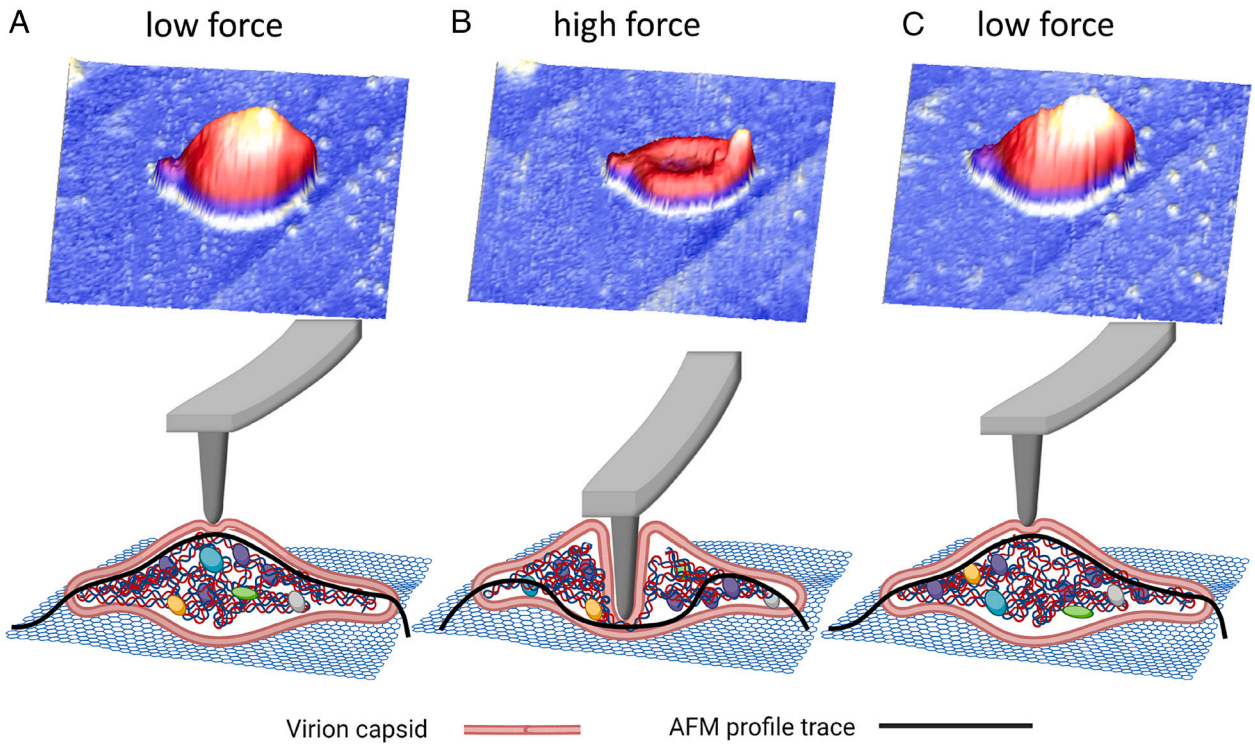

Fig. 6. Recreation of the SMV1 particle mechanical tomography. (*A*) SMV1 virus particle imaged at low force without presenting deformation (*Top*). The black line represents the apparent height profile at every pixel, which coincides with the actual virus topography (*Bottom*). (*B*) The same virus at high force (*Top*) shows a depressed apparent plateau (*Bottom*, black line) that forms only at the pixel where the tip is touching the virus (*Bottom*, capsid cartoon). (*C*) The same virus imaged again at low force (like in panel *A*) shows no apparent damage (*Top*). Again, the height profile at every pixel coincides with the actual virus topography (*Bottom*).

out not to participate in the capsid formation and instead was reassigned to the nucleoprotein core (16). In fact, our AFM topographies of dehydrated SMV1 particles (Fig. 5*B*) reveal a grainy structure around the collapsed virions, which is compatible with DNA bound by proteins, as we have previously observed in human adenovirus (41). The proposed packing fraction (11%) is probably a lower limit because of the effects of dehydration on the volume of core proteins and DNA. Nevertheless, if dehydration reduces the volume of proteins and dsDNA by half, the resulting packing fraction would be 22%, which still is very low compared with other viruses. In any case, it is evident that the low packing of SMV1 facilitates the SMV1 nucleoprotein fluidity.

SMV1 virions can undergo massive architectural rearrangements resulting in the development of one or two tails (64) that may be used to deliver the genome into the host. It has been hypothesized how unduloids used to model ATSV capsids (20) can store elastic energy in the structure while forming the bulge inside the virion, being able to withstand pressures up to 10 atmospheres (65). This transformation gradually yields virions that are 300% longer than the initial tail-less particles (18). Such reorganization is in stark contrast to other viruses with protein capsids, where the structural transformation due to maturation takes place in a single step and is far less dramatic. For instance, P22, Phi29, and HK97 bacteriophages increase their capsid sizes by just ~10%, showing stiffness 10 times larger than that of SMV1 and brittle fracture (25, 51, 66). The biomechanics of SMV1, exhibiting nucleocapsid fluidity and low stiffness, is likely to be linked to its enormous morphological plasticity, which would be inconceivable in the case of stiff and brittle capsids with positionally ordered capsid proteins (7, 67, 68). A theoretical model of the ATV capsid (20, 65) predicted the cargo to be an isotropic fluid which is able to double its density during tail growth. Dharmavaram et al. (20) proposed that archaeal lemon-shaped viruses are in a smectic liquid crystalline state that supports their transformation ability. They envisaged that the smectic state of the capsid undergoes large-scale changes without prohibitive energy penalty. Their predictions of the local elastic response against bulge formation are fully compatible with our experimental results. In addition, they showed that at mechanical equilibrium, besides the sphere and cylinder geometries, the shape of a "liquid" unduloid shell enclosing a volume under uniform pressure is expected to possess a surface of constant mean curvature.

The isotropic fluid nature of the cargo is consistent with the low packing fraction that we estimated for SMV1. Instead, unlike any other group of known viruses with protein capsids, SMV1 behaves as a "protein vesicle," being capable of high deformation and energy absorption driven by the shear between the shell and the fluid core and the high malleability of the capsid. Cryo-EM has revealed that SMV1 virion is built of seven helical filaments with hydrophobic interactions between them (16). Due to the nonspecific nature of hydrophobic interactions and lack of apparent contact between the capsid shell and the nucleoprotein cargo, as shown in the current study, these filaments can slide past each other to adapt the protein shell to the deformation induced by either the mechanical stress, as studied here, or during virion transformation into a tube which takes place in vivo (69). It is extensively described how the hydrophobic interactions can stabilize protein structures (70) for native oligomers such as vault particles or even for misfolded proteins (71, 72). Similar to SMV1 virions, vault particles can withstand mechanical fatigue and stress cycles and recover from mechanical assaults (73, 74). These molecular containers are also endorsed with a filamentous helicoid structure sustained by the hydrophobic interactions between protein filaments (75). Thus, the unique properties of the SMV1 virions can be explained by a combination of: i) the membrane-like protein

capsid which due to its inherent fluidity mediated by hydrophobic interactions, just like bona fide lipid membranes, has the ability to "heal" after mechanical assaults, and ii) the fluid nature of the nucleoprotein cargo, which unlike in other helical viruses, such as archaeal adnaviruses (10) or tobacco mosaic virus (76), is not fixed in the virion lumen through interaction with the capsid shell.

The SMV1 biomechanics may also have implications on its stability at high temperatures. For a harmonic oscillator with a spring constant k at temperature T, the thermal energy can be equated to the vibrational energy as $\frac{1}{2}k_BT = \frac{1}{2}k < x^2 >$ (77) where k_B is the Boltzmann's constant 1.38×10^{-23} J/K, $T = 348$ K (SMV1 growth temperature) and x the amplitude of vibration. For the sake of comparison, we can estimate the amplitude of vibration for human adenovirus and SMV1 at this temperature using their respective stiffness of 0.4 nN/nm (41) and 0.01 nN/nm (Fig. 2*C*) to be 1 Å and 7 Å, respectively. This results in vibrations of 1% and 7% of their size for adenovirus and SMV1 capsids, respectively. Therefore, SMV1 can better absorb the thermal vibrations than adenovirus, which in fact gets destabilized at 40 °C and disassembled at 45 °C (78), well below 75 °C.

Materials and Methods

SMV1 Cultivation and Purification. Sulfolobus monocaudavirus 1 (SMV1) was propagated in *Saccharolobus islandicus* CRISPR deletion mutant ΔC1C2 (79). The host cell culture was grown in Sulfolobus medium supplemented with 0.2% tryptone, 0.1% yeast extract, 0.2% sucrose, and 0.002% uracil (80).

The culture was started from a −80 °C stock. The cells were grown in 50 mL of medium at 76 °C with shaking. After 24 h of incubation, the cell culture was diluted 20 times in a prewarmed (76 °C) medium, and the growth was continued until the culture reached an OD_{600} of ~0.2. Then, the cells were infected with SMV1 stock, and incubation was continued at 76 °C with agitation for 24 h. The cells were removed by centrifugation (Sorvall 3000 rotor, 7,000 rpm, 20 min, 15 °C), virus-containing supernatant was collected, and virions precipitated with PEG6000 (10.5% w/v) and NaCl (5.8% w/v) for 2 h at room temperature. The PEG-precipitate was then pelleted (Sorvall 3000 rotor, 9,000 rpm, 30 min, 15 °C), and the resulting pellet was resuspended in one tenth of the original volume in 20 mM Tris–acetate (pH6) buffer.

The virus was purified by centrifugation (Beckman SW41 rotor, 38,000 rpm, at least 16 h, 15 °C) in CsCl density gradient (final CsCl concentration of 45% [w/v]). After the run, the opalescent band corresponding to SMV1 virions was collected. The purified SMV1 was stored in CsCl at 4 °C until used.

Atomic Force Microscopy. The sample was first diluted in TMS (50 mM Tris–HCl pH 7.2, 80 mM NaCl, and 20 mM $MgCl_2$) buffer and then applied into a freshly cleaved highly oriented pyrolytic graphite (HOPG ZYA Quality, Tipsnano, Kristiina 15-214, Tallinn, Estonia), incubated for 30 min, and then rinsed five times with the same buffer. All the experiments in liquid medium were carried out with NANOSENSORS™ qp-BioAC AFM probes, with a nominal tip radius smaller than 10 nm. The cantilevers were calibrated with Sader's method for rectangular cantilevers (81). The spring constants used for the experiments were 0.05 and 0.1 N/m. Rectangular silicon-nitride cantilevers (RC800PSA, Olympus, Center Valley, PA) with a nominal spring constant of 0.7 N/m were used in air AM-AFM experiments.

Measurements were carried out with a customized AFM (Nanotec Electrónica S.L.) using Jumping Plus Mode (54) and Amplitude Modulation AFM (AM-AFM) (82). In Jumping Plus Mode, lateral interactions are minimized as the lateral displacement is executed when the tip is far away from the sample. The tip moves perpendicularly to the surface (z direction) until reaching a certain cantilever bending. Once the topographical data are obtained, the tip releases the surface and is moved laterally one pixel to repeat the procedure again. In AM-dynamic mode, feedback is applied to the resonance frequency, and amplitude is modulated.

For the nanoindentation assays, individual particles were deformed with the AFM tip by performing single force-indentation curves (FIC) at a constant speed (50 nm/s). The first and second FICs were performed with a z piezo displacement of 150 nm. Thereafter, z piezo displacement was gradually increased to 200 and 300 nm. The elastic modulus of the particles was obtained from the linear regime of the FIC curves. Both breaking force and critical indentation were defined as the point at which a major drop in the normal force was obtained, usually after the end of the linear regime (29). All the images and curves were processed and analyzed using the WSxM software (83).

Data, Materials, and Software Availability. All study data are included in the article and/or supporting information.

ACKNOWLEDGMENTS. P.J.d.P. acknowledges grants from the Spanish Ministry of Innovation (FIS2017-89549-R; "Maria de Maeztu" Program for Units of Excellence in R&D MDM-2014-0377; and FIS2017-90701-REDT), PID2021-126608OB-I00, SI3/PJI/2021-00216, and from the Human Frontiers Science Program (HFSPO RGP0012/2018). The work in the M.K. laboratory was supported by a grant from Ville de Paris Emergence(s) program. Fig. 6 was made using biorender.com.

Author affiliations: [a]Departamento de Física de la Materia Condensada C03, Universidad Autónoma de Madrid, Madrid 28049, Spain; [b]Institut Pasteur, Université Paris Cité, Archaeal Virology Unit, Paris 75015, France; and [c]Instituto de Física de la Materia Condensada, Universidad Autónoma de Madrid, Madrid 28049, Spain

1. N. Dellas, J. C. Snyder, B. Bolduc, M. J. Young, Archaeal viruses: Diversity, replication, and structure. *Annu. Rev. Virol.* **1**, 399–426 (2014).
2. D. P. Baquero *et al.*, Structure and assembly of archaeal viruses. *Adv. Virus Res.* **108**, 127–164 (2020).
3. D. Prangishvili *et al.*, The enigmatic archaeal virosphere. *Nat. Rev. Microbiol.* **15**, 724–739 (2017).
4. R. Hartman, J. Munson-McGee, M. J. Young, C. M. Lawrence, Survey of high-resolution archaeal virus structures. *Curr. Opin. Virol.* **36**, 74–83 (2019).
5. M. Krupovic *et al.*, Adnaviria: A new realm for archaeal filamentous viruses with linear A-form double-stranded DNA genomes. *J. Virol.* **95**, e00673–21 (2021).
6. M. Krupovic, E. R. J. Quemin, D. H. Bamford, P. Forterre, D. Prangishvili, Unification of the globally distributed spindle-shaped viruses of the Archaea. *J. Virol.* **88**, 2354–2358 (2014).
7. R. Hochstein, D. Bollschweiler, H. Engelhardt, C. M. Lawrence, M. Young, Large tailed spindle viruses of archaea: A new way of doing viral business. *J. Virol.* **89**, 9146–9149 (2015).
8. C. Bath, M. L. Dyall-Smith, His1, an archaeal virus of the fuselloviridae family that infects haloarcula hispanica. *J. Virol.* **72**, 9392–9395 (1998).
9. M. Krupovic, V. V. Dolja, E. V. Koonin, The LUCA and its complex virome. *Nat. Rev. Microbiol.* **18**, 661–670 (2020).
10. F. Wang *et al.*, Structures of filamentous viruses infecting hyperthermophilic archaea explain DNA stabilization in extreme environments. *Proc. Natl. Acad. Sci. U.S.A.* **117**, 19643–19652 (2020).
11. F. DiMaio *et al.*, Virology. A virus that infects a hyperthermophile encapsidates A-form DNA. *Science* **348**, 914–917 (2015).
12. Y. Liu *et al.*, Structural conservation in a membrane-enveloped filamentous virus infecting a hyperthermophilic acidophile. *Nat. Commun.* **9**, 3360 (2018).
13. P. Kasson *et al.*, Model for a novel membrane envelope in a filamentous hyperthermophilic virus. *eLife* **6**, e26268 (2017).
14. K. B. Uldahl *et al.*, Recognition of extremophilic archaeal viruses by eukaryotic cells: A promising nanoplatform from the third domain of life. *Sci. Rep.* **6**, 37966 (2016).
15. D. Prangishvili, M. Krupovic, ICTV Report Consortium, ICTV virus taxonomy profile: Bicaudaviridae. *J. Gen. Virol.* **99**, 864–865 (2018).
16. F. Wang *et al.*, Spindle-shaped archaeal viruses evolved from rod-shaped ancestors to package a larger genome. *Cell* **185**, 1297–1307.e11 (2022).
17. M. Häring *et al.*, Virology: Independent virus development outside a host. *Nature* **436**, 1101–1102 (2005).
18. R. Hochstein *et al.*, Structural studies of *Acidianus* tailed spindle virus reveal a structural paradigm used in the assembly of spindle-shaped viruses. *Proc. Natl. Acad. Sci. U.S.A.* **115**, 2120–2125 (2018).
19. Z. Han *et al.*, Structural insights into a spindle-shaped archaeal virus with a sevenfold symmetrical tail. *Proc. Natl. Acad. Sci. U.S.A.* **119**, e2119439119 (2022).
20. S. Dharmavaram, J. Rudnick, C. M. Lawrence, R. F. Bruinsma, Smectic viral capsids and the aneurysm instability. *J. Phys. Cond. Matter* **30**, 204004 (2018).
21. K. B. Uldahl, S. T. Walk, S. C. Olshefsky, M. J. Young, X. Peng, SMV1, an extremely stable thermophilic virus platform for nanoparticle trafficking in the mammalian GI tract. *J. Appl. Microbiol.* **123**, 1286–1297 (2017).
22. P. Egan, R. Sinko, P. R. LeDuc, S. Keten, The role of mechanics in biological and bio-inspired systems. *Nat. Commun.* **6**, 7418 (2015).
23. M. G. Mateu, Assembly, stability and dynamics of virus capsids. *Arch. Biochem. Biophys.* **531**, 65–79 (2013).
24. A. Evilevitch, L. Lavelle, C. M. Knobler, E. Raspaud, W. M. Gelbart, Osmotic pressure inhibition of DNA ejection from phage. *Proc. Natl. Acad. Sci. U.S.A.* **100**, 9292–9295 (2003).
25. M. Hernando-Perez *et al.*, Direct measurement of phage phi29 stiffness provides evidence of internal pressure. *Small* **8**, 2366–2370 (2012).
26. V. González-Huici, M. Salas, J. M. Hermoso, The push–pull mechanism of bacteriophage Ø29 DNA injection. *Mol. Microbiol.* **52**, 529–540 (2004).

27. C. São-José, M. de Frutos, E. Raspaud, M. A. Santos, P. Tavares, Pressure built by DNA packing inside virions: Enough to drive DNA ejection in vitro, largely insufficient for delivery into the bacterial cytoplasm. *J. Mol. Biol.* **374**, 346–355 (2007).
28. W. H. Roos, AFM nanoindentation of protein shells, expanding the approach beyond viruses. *Semin. Cell Dev. Biol.* **73**, 145–152 (2018).
29. P. J. de Pablo, The application of atomic force microscopy for viruses and protein shells: Imaging and spectroscopy. *Adv. Virus Res.* **105**, 161–187 (2019).
30. N. Martin-Gonzalez *et al.*, Long-range cooperative disassembly and aging during adenovirus uncoating. *Phys. Rev. X* **11**, 021025 (2021).
31. M. Jimenez-Zaragoza *et al.*, Biophysical properties of single rotavirus particles account for the functions of protein shells in a multilayered virus. *Elife* **7**, e37295 (2018).
32. P. J. de Pablo, I. A. T. Schaap, Atomic force microscopy of viruses. *Phys. Virol. Virus Struct. Mech.* **1215**, 159–179 (2019).
33. S. Li, F. Eghiaian, C. Sieben, A. Herrmann, I. A. T. Schaap, Bending and puncturing the influenza lipid envelope. *Biophys. J.* **100**, 637–645 (2011).
34. B. Kiss, Z. Kis, B. Pályi, M. S. Z. Kellermayer, Topography, spike dynamics, and nanomechanics of individual native SARS-COV-2 virions. *Nano Lett.* **21**, 2675–2680 (2021).
35. M. Cantero, D. Carlero, F. J. Chichón, J. Martín-Benito, P. J. De Pablo, Monitoring SARS-CoV-2 surrogate TGEV individual virions structure survival under harsh physicochemical environments. *Cells* **11**, 1759 (2022).
36. J. S. Villarrubia, Algorithms for scanned probe microscope image simulation, surface reconstruction, and tip estimation. *J. Res. Natl. Inst. Stand. Technol.* **102**, 425–454 (1997).
37. C. Zeng *et al.*, Contact mechanics of a small icosahedral virus. *Phys. Rev. Lett.* **119**, 038102 (2017).
38. J. Snijder, I. L. Ivanovska, M. Baclayon, W. H. Roos, G. J. L. Wuite, Probing the impact of loading rate on the mechanical properties of viral nanoparticles. *Micron* **43**, 1343–1350 (2012).
39. A. Ortega-Esteban *et al.*, Monitoring dynamics of human adenovirus disassembly induced by mechanical fatigue. *Sci. Rep.* **3**, 1434 (2013).
40. C. Carrasco *et al.*, The capillarity of nanometric water menisci confined inside closed-geometry viral cages. *Proc. Natl. Acad. Sci. U.S.A.* **106**, 5475–5480 (2009).
41. N. Martin-Gonzalez *et al.*, Adenovirus major core protein condenses DNA in clusters and bundles, modulating genome release and capsid internal pressure. *Nucleic Acids Res.* **47**, 9231–9242 (2019).
42. A. Ortega-Esteban *et al.*, Mechanics of viral chromatin reveals the pressurization of human adenovirus. *ACS Nano* **9**, 10826–10833 (2015).
43. C. Carrasco, M. Castellanos, P. J. de Pablo, M. G. Mateu, Manipulation of the mechanical properties of a virus by protein engineering. *Proc. Natl. Acad. Sci. U.S.A.* **105**, 4150–4155 (2008).
44. H.-B. Pang *et al.*, Virion stiffness regulates immature HIV-1 entry. *Retrovirology* **10**, 4 (2013).
45. S. Azinas *et al.*, Membrane-containing virus particles exhibit the mechanics of a composite material for genome protection. *Nanoscale* **10**, 7769–7779 (2018).
46. A. Calò *et al.*, Force measurements on natural membrane nanovesicles reveal a composition-independent, high Young's modulus. *Nanoscale* **6**, 2275 (2014).
47. D. Vorselen, F. C. MacKintosh, W. H. Roos, G. J. L. Wuite, Competition between bending and internal pressure governs the mechanics of fluid nanovesicles. *ACS Nano* **11**, 2628–2636 (2017).
48. S. Dieluweit *et al.*, Mechanical properties of bare and protein-coated giant unilamellar phospholipid vesicles. A comparative study of micropipet aspiration and atomic force microscopy. *Langmuir* **26**, 11041–11049 (2010).
49. A. Ridolfi *et al.*, AFM-based high-throughput nanomechanical screening of single extracellular vesicles. *Anal. Chem.* **92**, 10274–10282 (2020).
50. M. Hernando-Pérez *et al.*, The interplay between mechanics and stability of viral cages. *Nanoscale* **6**, 2702–2709 (2014).
51. W. H. Roos *et al.*, Mechanics of bacteriophage maturation. *Proc. Natl. Acad. Sci. U.S.A.* **109**, 2342–2347 (2012).
52. D. Vorselen *et al.*, Multilamellar nanovesicles show distinct mechanical properties depending on their degree of lamellarity. *Nanoscale* **10**, 5318–5324 (2018).
53. A. Niknejad, S. A. Elahi, G. H. Liaghat, Experimental investigation on the lateral compression in the foam-filled circular tubes. *Mater. Des. 1980–2015* **36**, 24–34 (2012).
54. A. Ortega-Esteban *et al.*, Minimizing tip-sample forces in jumping mode atomic force microscopy in liquid. *Ultramicroscopy* **114**, 56–61 (2012).
55. L. R. Comolli *et al.*, Three-dimensional architecture of the bacteriophage phi29 packaged genome and elucidation of its packaging process. *Virology* **371**, 267–277 (2008).
56. U. Sae-Ueng *et al.*, Solid-to-fluid DNA transition inside HSV-1 capsid close to the temperature of infection. *Nat. Chem. Biol.* **10**, 861–867 (2014).
57. P. K. Purohit *et al.*, Forces during bacteriophage DNA packaging and ejection. *Biophys. J.* **88**, 851–866 (2005).
58. R. F. Bruinsma, G. J. L. Wuite, W. H. Roos, Physics of viral dynamics. *Nat. Rev. Phys.* **3**, 76–91 (2021).
59. P. K. Purohit, J. Kondev, R. Phillips, Mechanics of DNA packaging in viruses. *Proc. Natl. Acad. Sci. U.S.A.* **100**, 3173–3178 (2003).
60. F. Moreno-Herrero, J. Colchero, A. M. Baró, DNA height in scanning force microscopy. *Ultramicroscopy* **96**, 167–174 (2003).
61. S. Erdmann, R. A. Garrett, Selective and hyperactive uptake of foreign DNA by adaptive immune systems of an archaeon via two distinct mechanisms. *Mol. Microbiol.* **85**, 1044–1056 (2012).
62. P. Papathanasiou *et al.*, Stable maintenance of the rudivirus SIRV3 in a carrier state in *Sulfolobus islandicus* despite activation of the CRISPR-Cas immune response by a second virus SMV1. *RNA Biol.* **16**, 557–565 (2019).
63. S. Erdmann, S. Le Moine Bauer, R. A. Garrett, Inter-viral conflicts that exploit host CRISPR immune systems of *Sulfolobus*. *Mol. Microbiol.* **91**, 900–917 (2014).
64. K. B. Uldahl *et al.*, Life cycle characterization of sulfolobus monocaudavirus 1, an extremophilic spindle-shaped virus with extracellular tail development. *J. Virol.* **90**, 5693–5699 (2016).
65. L. E. Perotti *et al.*, Useful scars: Physics of the capsids of archaeal viruses. *Phys. Rev. E* **94**, 012404 (2016).
66. R. Kant *et al.*, Changes in the stability and biomechanics of P22 bacteriophage capsid during maturation. *Biochim. Biophys. ACTA-Gen. Subj.* **1862**, 1492–1504 (2018).
67. K. J. Hanhijärvi, G. Ziedaite, E. Hæggström, D. H. Bamford, Temperature and pH dependence of DNA ejection from archaeal lemon-shaped virus His1. *Eur. Biophys. J.* **45**, 435–442 (2016).
68. M. K. Pietilä, N. S. Atanasova, H. M. Oksanen, D. H. Bamford, Modified coat protein forms the flexible spindle-shaped virion of haloarchaeal virus His1: Relationships of short-tailed spindle-shaped viruses. *Environ. Microbiol.* **15**, 1674–1686 (2013).
69. E. R. J. Quemin *et al.*, Eukaryotic-like virus budding in archaea. *mBio* **7**, e01439–16 (2016).
70. S. Garde, Hydrophobic interactions in context. *Nature* **517**, 277–279 (2015).
71. N. Galamba, Aggregation of a Parkinson's disease-related peptide: When does urea weaken hydrophobic interactions? *ACS Chem. Neurosci.* **13**, 1769–1781 (2022).
72. M. Kieliszek, B. Lipinski, Pathophysiological significance of protein hydrophobic interactions: An emerging hypothesis. *Med. Hypotheses* **110**, 15–22 (2018).
73. A. Llauró *et al.*, Decrease in pH destabilizes individual vault nanocages by weakening the inter-protein lateral interaction. *Sci. Rep.* **6**, 34143 (2016), 10.1038/srep34143.
74. A. Llauró *et al.*, Mechanical stability and reversible fracture of vault particles. *Biophys. J.* **106**, 687–695 (2014).
75. P. Guerra *et al.*, Symmetry disruption commits vault particles to disassembly. *Sci. Adv.* **8**, eabj7795 (2022).
76. A. Klug, The tobacco mosaic virus particle: Structure and assembly. *Philos. Trans. R. Soc. Lond. B. Biol. Sci.* **354**, 531–535 (1999).
77. H.-J. Butt, M. Jaschke, Calculation of thermal noise in atomic force microscopy. *Nanotechnology* **6**, 1 (1995).
78. A. J. Perez-Berna *et al.*, The role of capsid maturation on adenovirus priming for sequential uncoating. *J. Biol. Chem.* **287**, 31582–31595 (2012).
79. S. Gudbergsdottir *et al.*, Dynamic properties of the Sulfolobus CRISPR/Cas and CRISPR/Cmr systems when challenged with vector-borne viral and plasmid genes and protospacers. *Mol. Microbiol.* **79**, 35–49 (2011).
80. W. Zillig *et al.*, Screening for sulfolobales, their plasmids and their viruses in icelandic solfataras. *Syst. Appl. Microbiol.* **16**, 609–628 (1993).
81. J. E. Sader, J. W. M. Chon, P. Mulvaney, Calibration of rectangular atomic force microscope cantilevers. *Rev. Sci. Instrum.* **70**, 3967–3969 (1999).
82. P. de Pablo, J. Colchero, M. Luna, J. Gomez-Herrero, A. Baro, Tip-sample interaction in tapping-mode scanning force microscopy. *Phys. Rev. B* **61**, 14179–14183 (2000).
83. I. Horcas *et al.*, WSXM: A software for scanning probe microscopy and a tool for nanotechnology. *Rev. Sci. Instrum.* **78**, 013705 (2007).